Original

Investigation of absorber and heterojunction in the pure sulphide kesterite

Charif Tamin [a,b,], Denis Chaumont [b], Olivier Heintz [b], Remi Chassagnon [b], Aymeric Leray [b], Nicolas Geoffroy [b], Maxime Guerineau [b], Mohamed Adnane [a]*

[a] *Laboratoire de Microscopie Electronique et Sciences des Matériaux (LMESM), Département de Technologie des Matériaux, Faculté de physique, Université des Sciences et de la Technologie d'Oran Mohamed Boudiaf USTO-MB, El M'naouar, BP 1505, Bir El Djir, 31000 Oran, Algeria*

[b] *Laboratoire Interdisciplinaire Carnot de Bourgogne (ICB), Université de Bourgogne Franche-Comté, BP 47 870, 21078 Dijon, France*

ARTICLE INFO

ABSTRACT

This paper aims to study the properties of the absorber layer and the heterojunction in kesterite solar cells. The Cu_2ZnSnS_4 (CZTS) thin films were layered on a glass substrate from a colloidal solution of metal salts and thiourea dissolved in a mixture of water and ethanol and deposited by spin coating technique. The samples were then heat treated in a furnace, in the presence of sulphur powder and under a nitrogen gas flow. The results revealed the formation of homogeneous layers of a pure kesterite phase of CZTS crystallites after heat treatment with correct stoichiometry and oxidation states. The optical transmission measurements indicate an energy band-gap of 1.4 eV and an absorption coefficient of 10^4 cm^{-1}. These CZTS thin films, elaborated by spin coating process, were integrated for electronic properties evaluation in a heterojunction in the following configuration: SnO$_2$:F (FTO) and Molybdenum as back contact, CdS as tampon and the CZTS film as absorber layer. The band alignment at the CdS–CZTS heterojunction indicates a cliff-like conduction band offset (CBO) even close to be a flat band.

© 2020 SECV. Published by Elsevier España, S.L.U. This is an open access article under the CC BY-NC-ND license (http://creativecommons.org/licenses/by-nc-nd/4.0/).

Investigación del absorbente y la heterojunción en el sulfuro puro kesterita

RESUMEN

Este trabajo tiene como objetivo estudiar las propiedades de la capa absorbente y la hetero-junción en las células solares de kesterita. Las finas películas de Cu_2ZnSnS_4 (CZTS) fueron colocadas en capas sobre un sustrato de vidrio a partir de una solución coloidal de sales metálicas y tiourea disueltas en una mezcla de agua y etanol, y depositadas mediante la técnica de revestimiento por centrifugado. A continuación las muestras se trataron térmi-camente en un horno, en presencia de polvo de azufre y bajo un flujo de gas nitrógeno. Los

---

* *Corresponding author.*
E-mail addresses: charif.tamin@univ-usto.dz, charif_tamin@etu.u-bourgogne.fr (C. Tamin).

resultados revelaron la formación de capas homogéneas de una fase de kesterita pura de los cristales de CZTS después del tratamiento térmico con la estequiometría y los estados de oxidación correctos. Las mediciones de la transmisión óptica indican una brecha en la banda de energía de 1,4 eV y un coeficiente de absorción de 10^4 cm^{-1}. Estas películas delgadas de CZTS, elaboradas por el proceso de revestimiento de espín, se integraron para la evaluación de las propiedades electrónicas en una heterojunción en la siguiente configuración: SnO$_2$: F (FTO) y molibdeno como contacto posterior, CdS como tampón y la película CZTS como capa absorbente. La alineación de la banda en la heterojunción CdS-CZTS indica un desplazamiento de la banda de conducción (CBO) similar al de un acantilado, incluso cerca de ser una banda plana.

Introduction

In recent years, photovoltaic energy has become a promising source for meeting the energy that society demands. Currently, silicon-based solar cells are the most commercialised product on the photovoltaic market. The expensive and polluting manufacturing techniques of crystalline silicon solar cells led scientists to find a new generation of solar cells that are more economical and environmentally friendly.

Thin-film solar cells are a promising alternative that could achieve this goal by reducing the amount of materials. In recent years, three thin-film solar cells technologies were developed: amorphous silicon (a-Si), cadmium telluride (CdTe) and CIGS (CuIn$_x$Ga$_{1-x}$Se$_2$). The CIGS technology achieved a higher efficiency (22.9%) than the cadmium telluride (21%) and amorphous silicon (10.2%) [1]. However, (CdTe) technology uses two toxic element (Cd and Te) and the CIGS technology involves the use of rare elements such as indium and gallium. In addition, indium is now widely used in touchscreen technology [2] and its price could significantly increase in the future and affect the production of the CIGS technology.

To avoid the use of toxic and rare elements, new material kesterite (Cu$_2$ZnSnS$_4$ or Cu$_2$ZnSnSe$_4$ referred as CZTS and CZTSe) using copper, zinc, tin, and sulphur or selenium elements, has attracted considerable interest in recent years and became promising for the development of eco-friendly solar cells. This compound is a p-type semiconductor and is therefore used as an absorber layer in solar cells. Its near-optimum direct band gap energy of 1.5 eV and its large absorption coefficient, greater than 10^4 cm^{-1}, make it one of the most promising materials for photovoltaic applications [3,4]. Although this innovative technology has grown rapidly in recent years, its performance is weak compared to CIGS. The best efficiency of kesterite solar cells is 12.6% for Cu$_2$ZnSn (S, Se)$_4$ and 10% for Cu$_2$ZnSnS$_4$ [1,5].

The development of kesterite solar cells is currently limited by the large open circuit voltage (V_{oc}) deficit [6,7]. This high V_{oc} deficit ($E_g/q - V_{oc}$) is strongly dependent on several factors, in particular related to the purity of the CZTS absorbent material and the quality and nature of the interfaces between the different layers and non-ideal band alignment that limits its charge separation at the absorber/tampon heterojunction [8–10]. Thus, the CZTS layer must be pure (without parasitic phases) and stable during the deposition and the heat treatment processes (no loss of tin and sulphur by evaporation or diffusion in the other layers of the cell). As well as, the heterojunction needs more investigations to understand the recombination limits at the heterojunction-interface absorber/buffer (CZTS/CdS), which is one of the main factors in addition to the absorbent layer problems limiting the efficiency.

Hence, obtaining a pure phase of CZTS required optimisation. The mechanism of formation of secondary phases and decomposition of CZTS phase during heat treatment is still under study [11]. Several authors have reported the presence of secondary phases in the kesterite structure, such as Cu$_{2-x}$S, SnS, SnS$_2$, Cu$_2$SnS$_3$, which are p-type or n-type semiconductors or insulators, that can form secondary diodes inside of the CZTS [11–13]. A review by Kuma et al. indicates that, under equilibrium conditions, a copper-rich layer can suppress the secondary phases and assist in the formation of the pure phase of CZTS [12]. Kermadi et al. proved that copper-rich CZTS could remove some secondary phases but was unable to remove the copper sulphide phase [14]. Ashfaq et al. recently demonstrated that the use of In$_2$O$_3$:Sn (ITO) substrate promotes the growth of a single-phase, namely CZTS [15]. However, most of the previous studies did not take into account the diffusion mechanisms when using ITO to obtain a single and pure CZTS phase: crystallographically the phase is kesterite but chemically, indium can partially substitute tin and form a Cu$_2$ZnSn$_{1-x}$In$_x$S$_4$ alloy (CZITS), which may changes the properties of the CZTS and promote the appearance of the In$_2$O$_3$ phase [16].

For the heterojunction engineering, an unoptimised hetero interface between the absorber and the buffer layer could result in a major limitation on device performance. However, the heterojunction engineering has achieved relatively little attention in the kesterite community. Recently, Yan et al. (2018) obtained the efficiency record of kesterite sulphide solar cells by heterojunction heat treatment [5]. Thus, further focused experimental investigations at the absorber-buffer hetero-interfaces will be impactful in the kesterite development.

In this paper, we present the deposition process and the optical, structural, and chemical characterisations of single phase kesterite on a glass substrate by spin coating and sulphurisation process. These CZTS thin films were used in a stack of layers to produce all solution heterojunction. The electronic properties of the CdS/CZTS het-

erojunction were collected experimentally by XPS including core-level, valance band positions and UV–visible bandgap measurements.

Experimental

CZTS thin films were deposited on substrates by spin coating and heat treated in a furnace under controlled atmosphere. The complete heterojunction was elaborated using chemical bath deposition and spin coating techniques. Various characterisation techniques were carried out to study the properties of CZTS thin films and heterojunctions.

CZTS thins films preparation

The colloidal solution was prepared by dissolving copper chloride dihydrate, zinc chloride, tin chloride dihydrate and thiourea (H_2NCSNH_2) with respective concentrations of 0.4 M, 0.2 M, 0.2 M and 1 M in a mix of water (75%) and ethanol (25%). Some drops of ethanolamine were added to the solution as stabiliser, where the pH of the solution was around 4. The solution was stirred for 6 h at room temperature to obtain a clear yellow-coloured colloidal solution.

CZTS thin films were layered on glass substrates from the colloidal water-ethanol solution by spin coating processing at 4000 rpm for 30 s. Samples were then dried directly on a hot plate heated at 250 °C for 10 min under air ambient. This process was repeated 10 times (for a final thickness of 1.2 μm). Samples were subsequently heat treated in a furnace at 520 °C during 30 min in the presence of sulphur (0.5 g) under nitrogen gas flow.

Samples CTB01 and CTB01S respectively correspond to the CZTS thin films before and after heat treatment.

Heterojunction fabrication

The heterojunction prototype was built as follows:

- The first layer was Molybdenum (Mo). This Mo layer was deposited using an e-beam evaporator (Plassys MEB400) on FTO (fluorine-doped tin oxide, SnO_2:F) glass substrates provided by SOLEM Company. The thickness of the Mo layer was 100 nm;
- The second layer was the CZTS (5 layers) thin film deposited using a spin coating technique as described above (CZTS thins films preparation section);
- The third layer was the CdS buffer layer deposited by Chemical Bath Deposition CBD (70 °C, 15 min). The chemical bath composition was: 20 mL of deionised water, 5 mL of 0.1 M $CdCl_2$, 20 mL of 0.1 M thiourea and 17.5 mL of 6.5 M NH_4OH. The pH of the chemical bath during the reaction was about 10.

This stack of layers will be referred to as HJ19-01. Finally, a rapid annealing was performed in a furnace at 270 °C for 10 min under nitrogen gas flow without sulphur. The as-built heterojunction will be labelled as HJ19-01S.

Characterisations

Transmission Electron Microscopy (TEM) was performed on a JEOL JEM-2100F microscope to characterise the CZTS thin film microstructure. For the preparation, thin films were removed from the substrate by scratching them with a scalpel. Afterwards, the sample surface is wiped with a carbon-coated gold grid, resulting in pieces of the films stuck to the carbon film. The local morphology and the crystallography were studied using conventional, high resolution microscopy (HRTEM) and Selected Area Electron Diffraction (SAED) modes.

The surface morphology (Plain view) and the multilayer stack (cross-section) of the heterojunction were examined by Scanning Electron Microscopy (SEM). The observations were performed on a Hitachi SU8230 SEM equipped with an Energy Dispersive Spectrometer (Thermo Scientific NSS SDD) allowing chemical analyses of the films.

The atomic states, chemical compositions and valence band data were determined by X-ray Photoelectron Spectroscopy (XPS) and performed using a PHI Versaprobe 5000 apparatus with monochromated Al $K\alpha_1$ X-rays (energy of 1486.6 eV, power of 50 W and X-ray spot diameter of 200 μm). Experiments were realised after sputtering of the CTB01, CTB01S and HJ19-01S samples in order to remove the major part of the thin layer of oxide from atmospheric contamination. Sputtering was done with argon ions of 500 eV for 5 min for the thin films (incidence angle of 45°). For the heterojunction, the XPS data were collected after each 60 s of etching time. In this condition, the sputtering rate of standard silicon dioxide is around 2 nm/min. Adventitious carbon from atmospheric pollution is used as internal standard for energy calibration (1s level at 284.8 eV). During measurements, the residual pressure of the analysis chamber was maintained below 10^{-7} Pa. Spectra were processed with the Casa software package and the ionisation cross-sections from Landau model were used in order to quantify the semi-empirical relative sensitivity factors.

The crystallographic structures of samples was investigated by X-Ray Diffraction (XRD) and performed with a Bruker D8 DISCOVER (CuKα radiation source λ = 1.5406 Å).

The size of nanocrystals was estimated from the Scherrer formula [17]:

$$D_{hkl} = 0.89\lambda/B_{hkl}\cos\theta$$

where λ is the X-ray wavelength used, B_{hkl} the full width at half maximum and θ the Bragg angle of the studied peak.

The Raman spectroscopy (Raman) was performed with a custom-built epi-confocal microscope equipped with a 40× objective lens (0.6 NA, Nikon). The sample was illuminated with a laser excitation wavelength of 784 nm and an intensity of 0.6 mW at the focus. Raman spectra were acquired with a spectrometer (equipped with a grating of 1200 lines/mm) associated with a cooled CCD camera (1024×256 pixels). An exposition time of 10 s was used and the calibration was performed using a (111) silicon wafer at 520 cm^{-1}.

The Ultraviolet–visible Spectroscopy (UV–vis) was performed with a Thermo Spectronic Helios Gamma spectrophotometer, in the wavelength range 190–1100 nm with a 0.5 nm
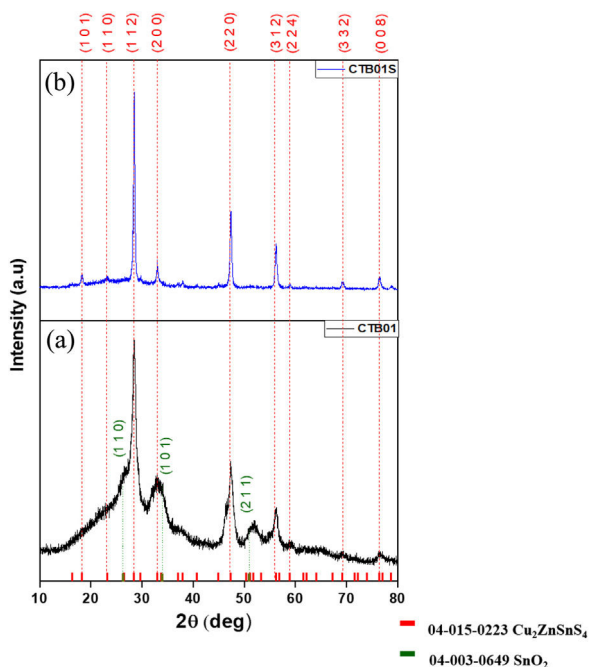
Fig. 1 – XRD diffractograms of the CZTS thin film, (a) raw sample CTB01, (b) heat treated sample CTB01S.

step to record the transmittance of thin films and to calculate the absorption coefficient, α, from the following equation:

$$\alpha = \frac{1}{e}\ln\left(\frac{1}{T}\right)$$

where e is the film thickness and T the transmittance [18]. Noted that the film thickness was measured using a Dektak 6 M Profilometer (Veeco).

The optical band gap values were determined using the Tauc diagram [16] where $(\alpha h\upsilon)^2$ is plotted as a function of the energy $h\upsilon$. The value of the gap is that at the intersection of the extrapolation of the linear part of the curve with the abscissa axis.

Results and discussion

Crystallographic and chemical characterisation

The XRD diffractogram of the CZTS layer before heat treatment (CTB01) is showed in Fig. 1a. The three major peaks at 28.43°, 47.27° and 56.15° are respectively assigned to the (112), (220) and (312) crystallographic planes of the kesterite tetragonal structure of CZTS (PDF card #04-015-0223). In addition to the CZTS major phase, the SnO_2 cassiterite phase is also detected, see peaks (110), (101) and (211) at respective angles 26.49°, 33.77° and 51.72° (PDF card #04-003-0649). This SnO_2 phase emerges during the drying process in ambient air on the hot plate.

The size of the nanocrystals, derived from the Scherrer formula, varies from 5.5 nm to 8.8 nm for each peak.

The XRD pattern of the annealed CZTS layer, CTB01S (Fig. 1b) shows narrow and intense diffraction peaks corresponding to the pure kesterite CZTS structure without

secondary phase. The cassiterite peaks have disappeared during annealing. Tin dioxide can turn into solid tin monosulphide [19,20] during annealing under sulphur atmosphere and tin monosulphide is a volatile specie above 500 °C [21].

The size of the nano-crystallites varied between 18.7 nm and 23.1 nm depending on the chosen peak. The peak intensities highlight an isotropic growth of the crystallites. Logically, the crystallites size increases under heat treatment.

The heat treatment under sulphur and nitrogen gas flow (oxygen free) prevents the formation of oxidised phases, increases the crystallisation, and helps the formation of the CZTS kesterite phase. In some case, as it seems to be the case here, it also avoids the decomposition of this structure into binary and ternary compounds such as $Cu_{2-x}S$, SnS_2, ZnS, Cu_2SnS_3 which has been observed by several authors in the literature [11–13].

In order to confirm the absence of secondary structures (as ZnS and Cu_2SnS_3, for which the three mains X-ray diffraction peaks are identical to CZTS ones), the SAED technique, the Fast Fourier Transformation of HRTEM image and the Raman spectroscopy were complementary performed.

Fig. 2(a, b) shows one electron diffraction patterns and the Fast Fourier Transformation of a High-Resolution image (HRTEM) of sample CTB01. The calculation of d spacing (Table 1) from the SAED confirm the results of XRD. Only pure Cu_2ZnSnS_4 kesterite crystallites were found in the studied samples. Fig. 2c shows where the SAED at the chemical analysis (EDS) were performed. The chemical composition in this area (Fig. 2d) shows the presence of four elements of the CZTS compound: copper, zinc, tin, and sulphur.

Fig. 3a shows the Raman spectrum of the CTB01 sample. The strongest peak at 335 cm^{-1} corresponds to the A mode of the kesterite structure of CZTS which is theoretically reported by Gurel et al. [22]. The weak peak at 363 cm^{-1} is assigned to the E (LO) mode of kesterite structure of CZTS [23]. For the calcined CTB01S sample (Fig. 3b), the peaks at 287 cm^{-1} and 337 cm^{-1} are assigned to the two A modes of the kesterite structure as well as the peaks at 366 cm^{-1} and 373 cm^{-1} which corresponds to the E(LO) and B(LO) modes [24–26]. The new intense peak at 287 cm^{-1}, may due to a better crystallinity of CTB01S compared to CTB01. As no other peaks are observed neither the ZnS (at 348 cm^{-1}) nor the $Cu_{2-x}S$ (at 476 cm^{-1}), SnS_2 at (315 cm^{-1}) and Cu_2SnS_3 (at 352 cm^{-1}) phases are present [27–32].

The different oxidation states were measured by XPS before and after etching for the CTB01 and CTB01S samples (see Fig. 4).

XPS spectra in Fig. 4a show the binding energy of Cu 2p$_{3/2}$ and Cu 2p$_{1/2}$ core levels, respectively at around 932 and 952 eV, for the raw and annealed CZTS samples. The measured binding energy for the Cu 2p$_{3/2}$ level and the absence of satellite at high binding energy for both peaks corroborate the Cu(I) oxidation state of copper in the whole CZTS layers [33–35].

The binding energy value of about 1021.8 eV for Zn 2p3/2 core level confirms the presence of Zn(II) for both CZTS layers, before and after calcination (see Fig. 4b) [35].

The Sn 3d$_{5/2}$ level for CTB01 and CTB01S samples are shown in Fig. 4c. Energy of this level slightly above 486 eV confirms the presence of Sn^{4+} species in the two samples [35,36].
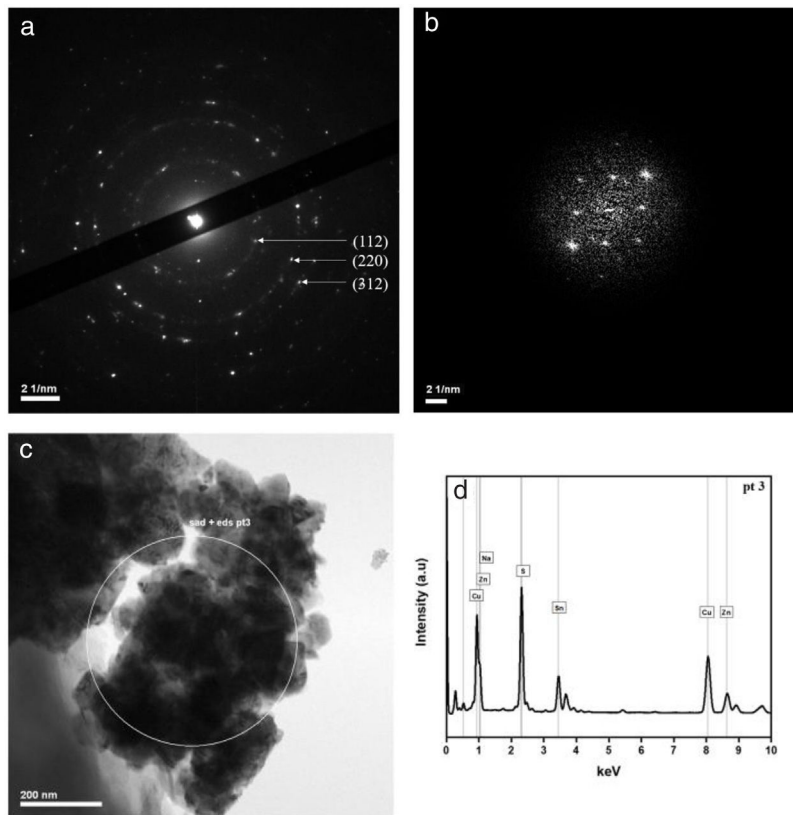
Fig. 2 – (a) Selected area electron diffraction pattern of the area shown in image (c); (b) fast Fourier transformation of a high-resolution image (HRTEM); (c) area of SAED and EDS acquisition; (d) energy dispersive spectroscopy (EDS) spectrum of image.

Table 1 – d-Spacing calculated from the selected area electron diffraction (SAED) and the associated diffraction planes.

Sample	d-Spacing (nm) SAED[a]	hkl planes[b]	Cu_2ZnSnS_4[c] PDF#04-015-0223	$\left\| d_{exp} - d_{th}/d_{th} \right\|$[d]
CTB01	0.3126	(112)	0.3134	0.26%
	0.1926	(220)	0.1919	0.36%
	0.1638	(312)	0.1636	0.12%
CTB01S	0.3132	(112)	0.3134	0.06%
	0.1916	(220)	0.1919	0.16%
	0.1632	(312)	0.1636	0.24%

[a] Experimental d-spacing.
[b] Diffraction planes.
[c] Theoretical d-spacing extracted from PDF#04-015-0223.
[d] Absolute errors.

Table 2 – Chemical compositions of the CZTS thin films analysed by energy dispersive spectroscopy EDS.

Sample	Cu	Zn	Sn	S	Cu/(Zn + Sn)	S/(Cu + Zn + Sn)
Atom %						
CTB01	36.05	17.25	16.60	30.09	1.064	0.43
CTB01S	27.61	11.88	13.75	46.76	1.077	0.88

Fig. 4d shows the XPS results for the sulphur species. The $2p_{3/2}$–$2p_{1/2}$ doublet could be separated in two distinct peaks: one centred near 162 eV, the other near 163 eV. The component at high binding energy 168 eV corresponds to sulphate SO_4^{2-} which decreases during sputtering but still detected after sputtering. The bulk component at low energy is assigned to the S^{2-} sulphur specie [37].

The chemical composition was also determined by EDS analyses for CTB01 and CTB01S samples (Table 2). The theoretical atomic composition of CZTS samples is respectively
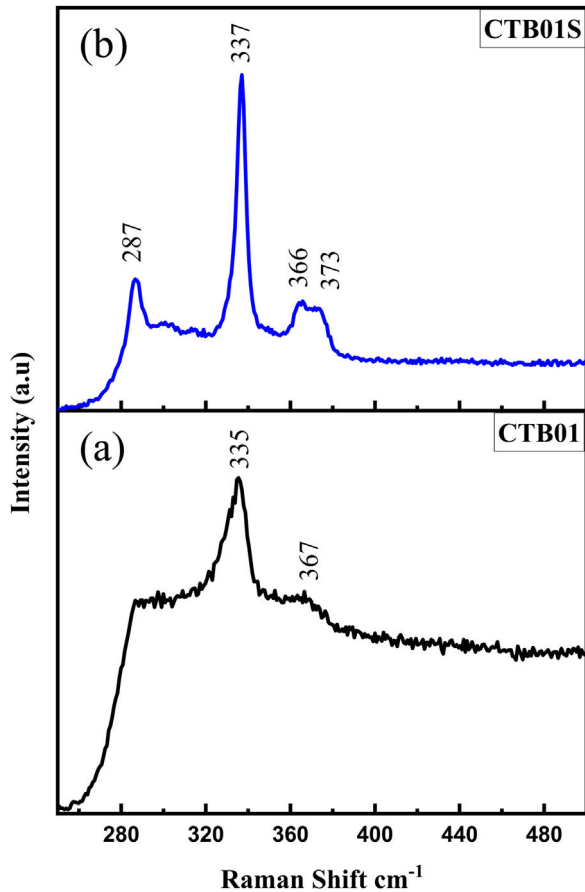
Fig. 3 – Raman spectra of the CZTS thin films. (a) As deposited sample CTB01, (b) heat treated sample CTB01S.

evaporation during the drying process after each deposition cycle. This ratio increases almost to 0.9 after annealing. This indicates that annealing under sulphur atmosphere allows to fill the sulphur vacancies and reach the Cu_2ZnSnS_4 stoichiometry.

From XPS analysis we can conclude that Cu(I), Zn(II), Sn(IV) and S(-II) are present in each sample. The formula Cu_2ZnSnS_4 is then consistent with XPS analysis and atomic concentrations obtained by EDS.

In conclusion, there is a good match between XRD analysis, electronic diffraction, Raman measurements, XPS analysis, and Energy Dispersive Spectroscopy which indicate the achievement of near stoichiometric CZTS of pure kesterite phase and required oxidation states.

Microstructural characterisation

Fig. 5(a–d) shows SEM images of the top view of CZTS thin films before CTB01 and after CTB01S heat treatment with different magnifications. Fig. 5(a, b) at low magnification (3000×) show a homogeneous surface without cracks for both CTB01 and CTB01S samples. Fig. 5(c, d) are at higher magnification (30 000×). CTB01S shows a larger grain size compared to CTB01.

Fig. 5(e–f) shows the SEM cross-section image of sample HJ19-01S and the corresponding EDS spectra of the different layers of the stack but acquired in STEM-EDS mode. New configuration was used to fabricate the heterojunction by employing FTO/Mo as a back contact (*Heterojunction fabrication* section). This new design allows to reduce the thickness of interfacial layer MoS_2 during heat treatment. In fact, a relatively thick layer of MoS_2 forms a Schottky-type barrier and favourite the decomposition of absorber layer in CZTS solar cells [18,6].

According to the SEM image, the thickness of the back contact is approximately 400 nm for FTO and 150 nm for Mo/MoS_2. The thickness of the absorber (CZTS) and the buffer (CdS) are almost 560 nm and 90 nm respectively. In the absorber layer, we notice the existence of two layers
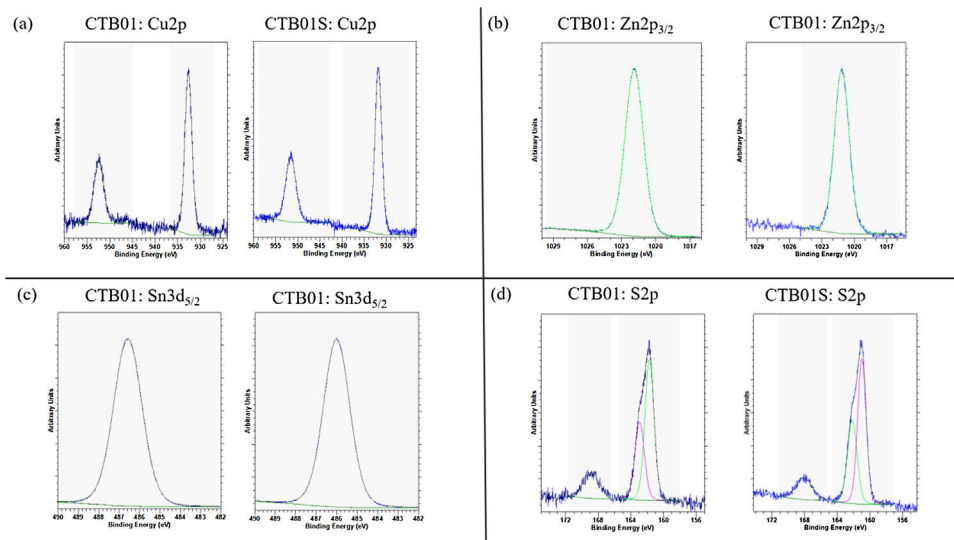
25, 12.5, 12.5 and 50 percent for copper, zinc, tin and sulphur. The ratio Cu/(Zn + Sn) remains close to 1 for both samples and is the stoichiometric expected value. On the other hand, the S/(Cu + Zn + Sn) ratio of about 0.4 for sample CTB01 is very low compared to the theoretical one of 1. This could be due to the
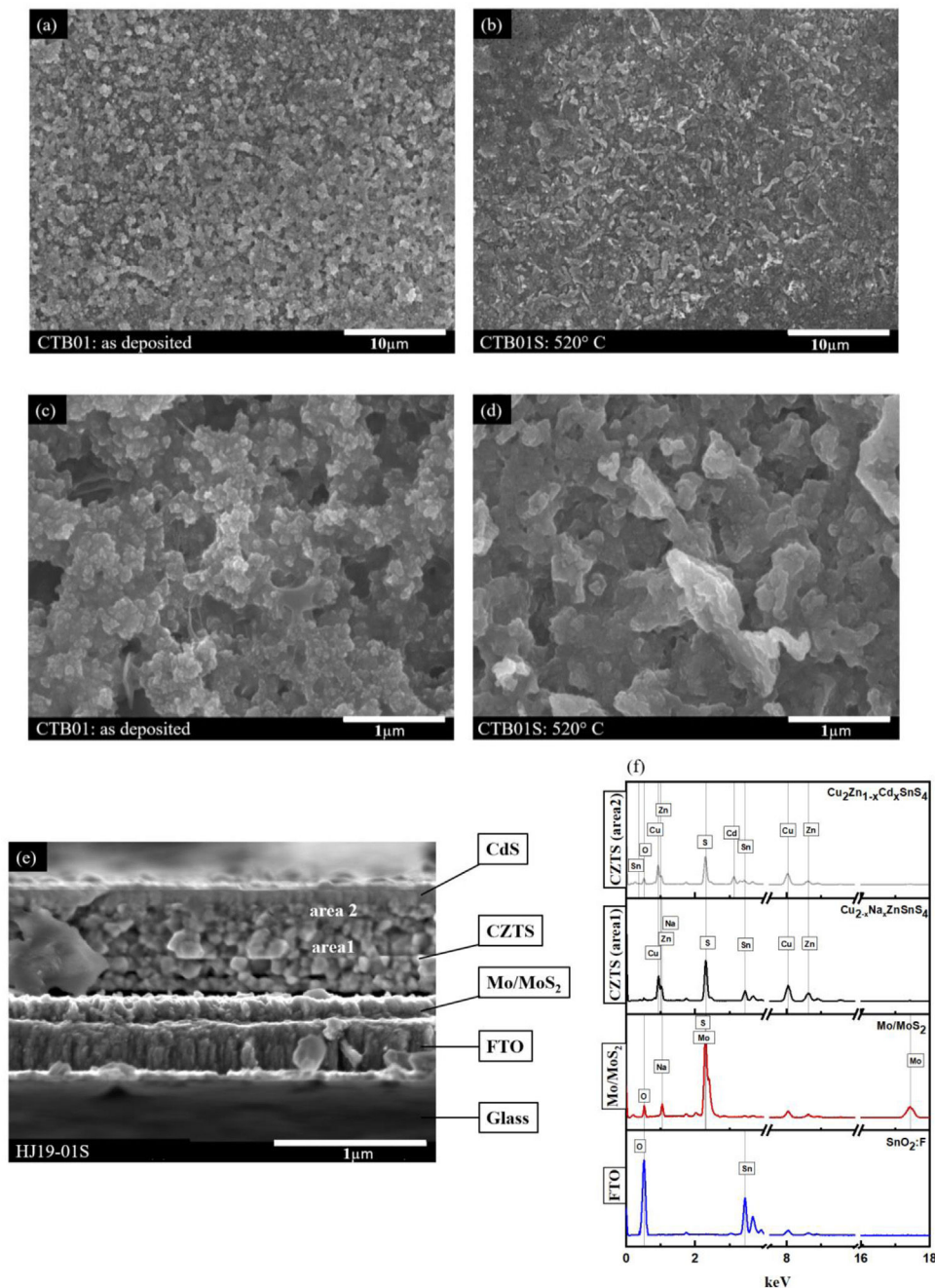

Fig. 4 – XPS spectra of the CZTS thin films before and after heat treatment. (a) Cu2p, (b) Zn2p3/2, (c) Sn3d5/2 and (d) S2p.

Fig. 5 – SEM micrographs of the CZTS thin films. (a–c) As deposited sample CTB01, (b–d) after heat treatment sample CTB01S. (e) SEM cross-section image of the heterojunction prototype HJ1901S. (f) EDS analysis across the heterojunction HJ1901S (in scanning TEM mode).

of different morphology: one with large grains on the bulk side and the other with smaller grains on the surface side of the CZTS. This last layer is close to the CZTS-CdS interface. According to the EDS analysis in Fig. 5(f) this variation due to the diffusion of Cd into the CZTS absorber layer.

Optical measurements

Fig. 6a shows the transmittance spectrum of CZTS samples before (CTB01) and after (CTB01S) heat treatment. The curve indicates that both layers have a low transmittance in the range 200–1100 nm, which mean high photons absorption by the CZTS layers. In addition, over the area 300 nm to 400 nm and 800–1100 nm, the transmittance for CTB01S is higher than CTB01. However, above 450–800 nm the transmittance decreases for the heat-treated sample CTB01S.

Fig. 6(b–e) shows the band gaps and absorption coefficient as a function of energy for the two samples CTB01 and CTB01S. The band gap of CTB01 is about 1.5 eV and the absorption coefficient is estimated to be 3.3×10^4 cm^{-1} at 1.5 eV and
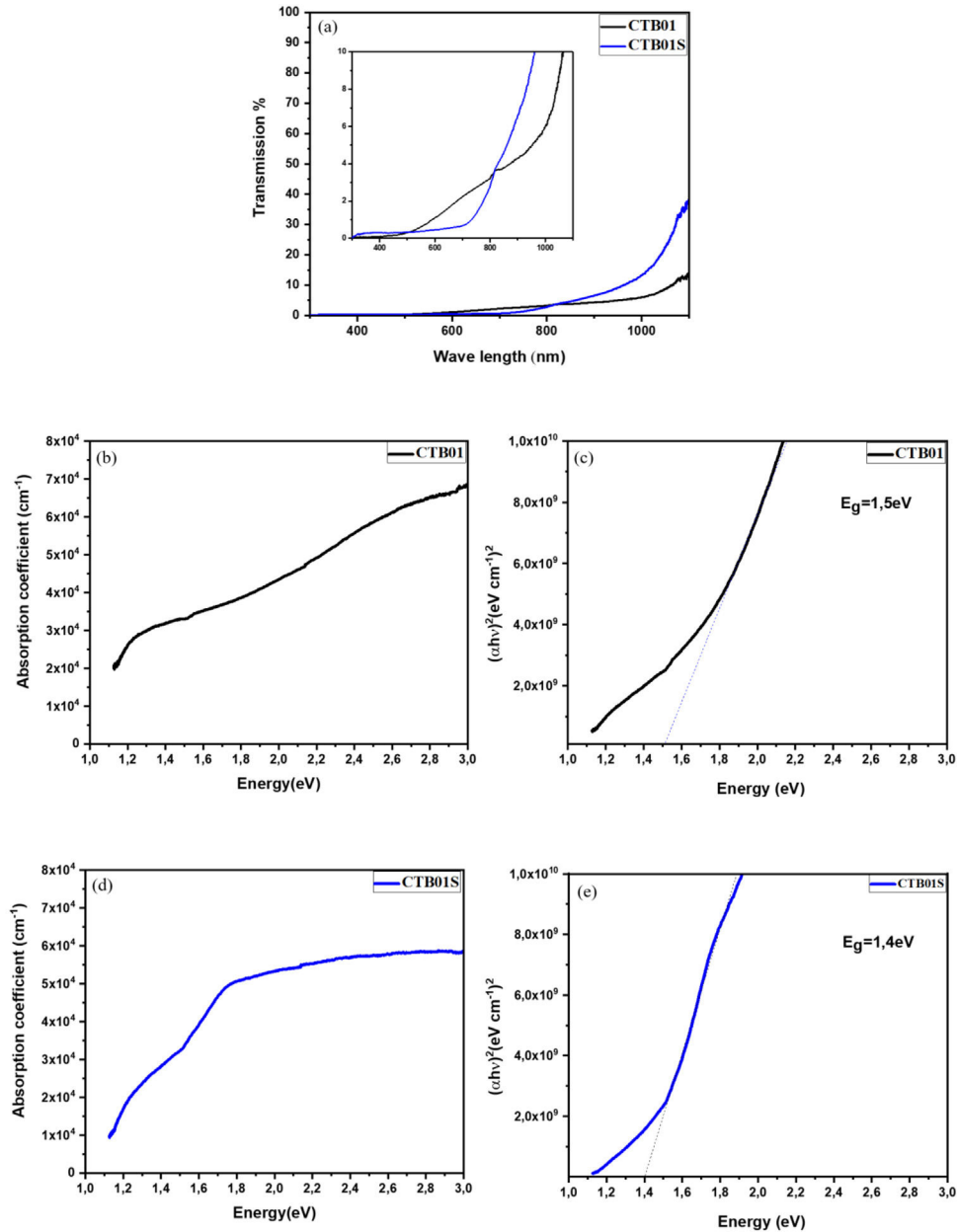
Fig. 6 – (a) Transmittance of the CZTS thin films; absorption coefficient of the CZTS thin films as a function of energy, (b) as deposited sample CTB01, (c) sample after heat treatment CTB01S; optical band gap of the CZTS thin films (d) CTB01 and (e) CTB01S.

5.8×10^4 cm^{-1} at 3 eV. The band gap of CTB01S decrease after heat treatment to be 1.4 eV, the absorption coefficient at this value was estimated to be 2.8×10^4 cm^{-1} and 5.6×10^4 cm^{-1} at 3 eV. However, there is a second optical transition below the bandgap for both samples, which may due to tail states [38,39].

As results, the absorption coefficient of 10^4 cm^{-1} and the band gap range of about 1.4 eV to 1.5 eV for the heat-treated layers CZTS make these films suitable to be incorporated as an absorber layer for thin films solar cells. This is consistent with several theoretical and experimental studies [3,4,40].

Heterojunction engineering

The electronic characterisation of CdS/CZTS heterojunction was determined from XPS depth profile measurements including valence band (VB) and core level (CL). A low-energy argon sputtering was applied from the upper CdS layer to the lower
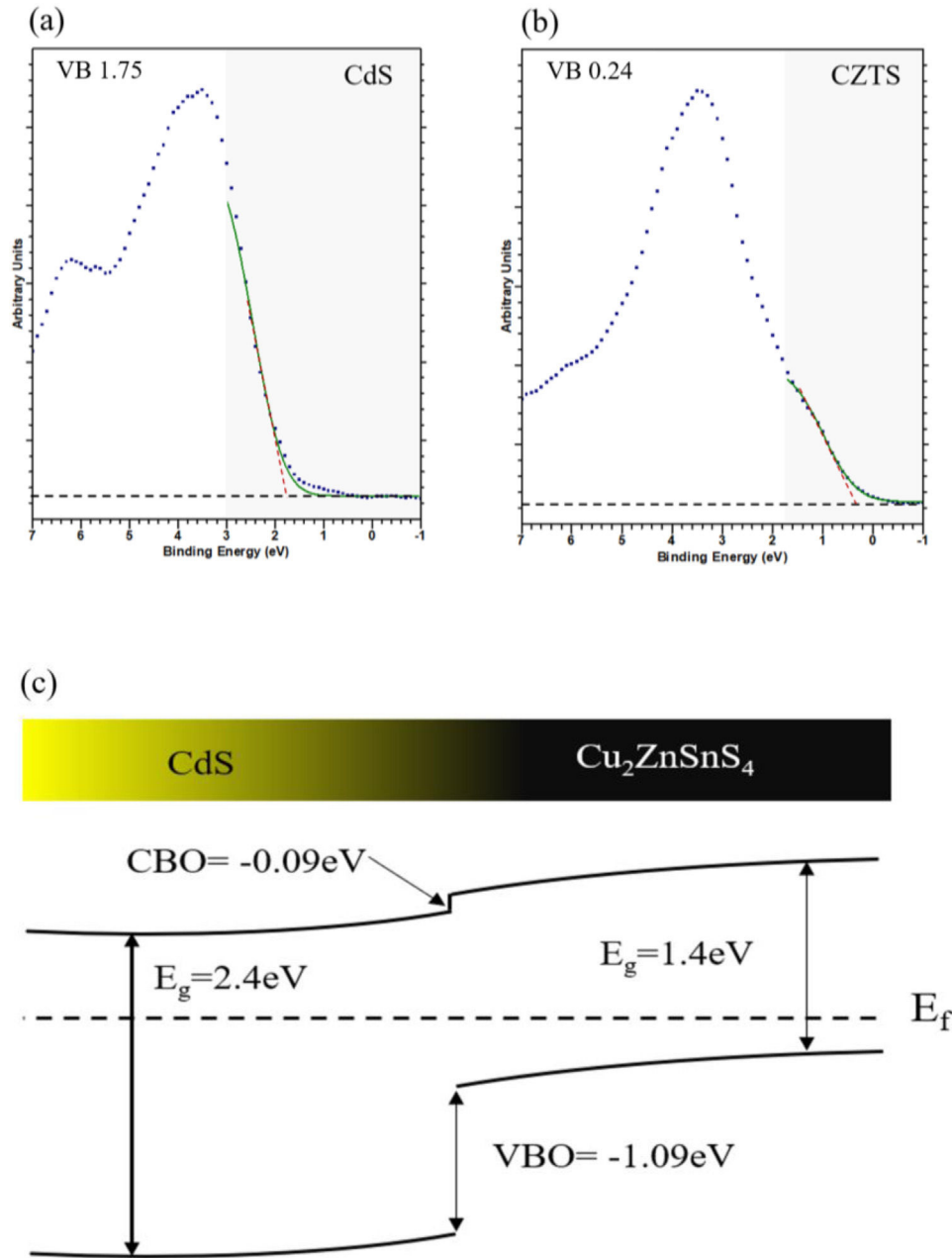
Fig. 7 – XPS valence band spectrum for bulk CdS (a) and CZTS(b). (c) Band alignment at CdS–CZTS heterojunction.

CZTS layer passing through the hetero-interface. In this way it is possible to access the values of core level energy used to determine the band bending (V_{bb}) both in bulk and at the interface. Based on Kaut formula shown in Eq. (1) [41–43], the (V_{bb}) value equals to 0.42 eV.

$$V_{bb} = \left[\left(E_{CL}^a - E_{CL}^a(i) \right) + \left(E_{CL}^b(i) - E_{CL}^b \right) \right] \tag{1}$$

where E_{CL}^a and E_{CL}^b are the core level energies of two selected elements in the CdS and CZTS bulk respectively, $E_{CL}^a(i)$ and $E_{CL}^b(i)$ are the same core level energies measured at interface.

Measurements on VB region are done between -1 and 7 eV (assuming BE at 0 eV represent the energy of fermi level energy E_f and the bending energy below 0 eV was negative) for pure

CdS (Fig. 7a) and pure CZTS (Fig. 7b). The VB positions were estimated by extrapolation of the linear slope in the VB spectra near E_f. In this way the VB position of the bulk materials are about -1.75 eV for CdS and -0.24 eV for CZTS.

The band alignment at the heterojunction, was estimated using the indirect method by applying the valance band offset (VBO) and Conduction band offset (CBO) values. The VBO was deduced from the VB positions and the band bending as shown in Eq. (2). The CBO was calculated by adding the optical band offset of CdS–CZTS to the VBO value as indicated in Eq. (3).

$$VBO = E_b^{VB} - E_a^{VB} + V_{bb} \tag{2}$$

$$CBO = \left(E_g{}^{CdS} - E_g{}^{CZTS} \right) + VBO \tag{3}$$

where E_b^{VB} and E_a^{VB} represent the valence band energy of CZTS and CdS respectively.

Fig. 7c shows the band alignment at CdS–CZTS heterojunction where VBO is about $-1.09\,eV$ and CBO about $-0.09\,eV$ which indicate small cliff like CBO close to be flat band. These results indicate good alignment of the heterojunction CdS–CZTS, which can improve the efficiency of pure sulphide Kesterite devices.

Conclusion

CZTS thin films were successfully deposited by spin coating from a colloidal solution. The characterisation results show that the CZTS thin films deposited by spin coating and sulphurised at $520\,^{\circ}C$ with solid sulphur under nitrogen ambient, are of pure kesterite structure of Cu_2ZnSnS_4 with the proper oxidation states. The optical band gap of $1.4\,eV$ and the absorption coefficient greater than $10^4\,cm^{-1}$ seem ideal for an absorbent layer in solar cells.

The heterojunction indicates a good band alignment by heat treatment of the heterojunction which indicates a cliff like CBO even close to being a flat band. As a result, it can facilitate charge separation and improve the efficiency of pure sulphide kesterite devices.

Acknowledgement

REFERENCES

[1] M.A. Green, E.D. Dunlop, D.H. Levi, J. Hohl-Ebinger, M. Yoshita, A.W.Y. Ho-Baillie, Solar cell efficiency tables (version 54), Prog. Photovolt Res. Appl. 27 (2019) 565–575, http://dx.doi.org/10.1002/pip.3171.

[2] C.N. Mercer, Indium—bringing liquid-crystal displays into focus: U.S. Geological Survey Fact Sheet 2015-3012, 2015, pp. 2, http://dx.doi.org/10.3133/fs20153012.

[3] H. Katagiri, Cu2ZnSnS4 thin film solar cells, Thin Solid Films 480–481 (2005) 426–432, http://dx.doi.org/10.1016/j.tsf.2004.11.024.

[4] S.C. Riha, B.A. Parkinson, A.L. Prieto, Solution-based synthesis and characterization of Cu_2ZnSnS_4 nanocrystals, J. Am. Chem. Soc. 131 (2009) 12054–12055, http://dx.doi.org/10.1021/ja9044168.

[5] C. Yan, J. Huang, K. Sun, S. Johnston, Y. Zhang, H. Sun, A. Pu, M. He, F. Liu, K. Eder, L. Yang, J.M. Cairney, N.J. Ekins-Daukes, Z. Hameiri, J.A. Stride, S. Chen, M.A. Green, X. Hao, Cu2ZnSnS4 solar cells with over 10% power conversion efficiency enabled by heterojunction heat treatment, Nat. Energy 3 (2018) 764–772, http://dx.doi.org/10.1038/s41560-018-0206-0.

[6] X. Liu, Y. Feng, H. Cui, F. Liu, X. Hao, G. Conibeer, D.B. Mitzi, M. Green, The current status and future prospects of kesterite solar cells: a brief review: kesterite solar cells, Prog. Photovolt: Res. Appl. 24 (2016) 879–898, http://dx.doi.org/10.1002/pip.2741.

[7] M. Neuschitzer, S. Giraldo, J. Marquez, M. Dimitrievska, M. Placidi, I. Forbes, V. Izquierdo-Roca, A. Perez-Rodriguez, E. Saucedo, Enhancing grain growth and boosting Voc in CZTSe absorber layers — Is Ge doping the answer? in: 2016 IEEE 43rd Photovoltaic Specialists Conference (PVSC), IEEE, Portland, OR, USA, 2016, pp. 0183–0187, http://dx.doi.org/10.1109/PVS.C.2016.7749574.

[8] L. Grenet, M.A.A. Suzon, F. Emieux, F. Roux, Analysis of failure modes in kesterite solar cells ACS Appl. Energy Mater. 1 (2018) 2103–2113, http://dx.doi.org/10.1021/acsaem.8b00194.

[9] M. Courel, J.A. Andrade-Arvizu, O. Vigil-Galán, Loss mechanisms influence on Cu_2ZnSnS_4/CdS-based thin film solar cell performance, Solid-State Electron. 111 (2015) 243–250, http://dx.doi.org/10.1016/j.sse.2015.05.038.

[10] M. Courel, J.A. Andrade-Arvizu, O. Vigil-Galán, Towards a CdS/Cu_2ZnSnS_4 solar cell efficiency improvement: a theoretical approach, Appl. Phys. Lett. 105 (2014) 233501, http://dx.doi.org/10.1063/1.4903826.

[11] G. Chen, W. Wang, J. Zhang, S. Chen, Z. Huang, Formation mechanism of secondary phases in Cu_2ZnSnS_4 growth under different copper content, Mater. Lett. 186 (2017) 98–101, http://dx.doi.org/10.1016/j.matlet.2016.09.090.

[12] M. Kumar, A. Dubey, N. Adhikari, S. Venkatesan, Q. Qiao, Strategic review of secondary phases, defects and defect-complexes in kesterite CZTS–Se solar cells, Energy Environ. Sci. 8 (2015) 3134–3159, http://dx.doi.org/10.1039/C5EE02153G.

[13] D.M. Berg, P.J. Dale, Kesterites: equilibria and secondary phase identification, in: K. Ito (Ed.), Copper Zinc Tin Sulfide-Based Thin-Film Solar Cells, John Wiley & Sons Ltd, Chichester, UK, 2015, pp. 107–132, http://dx.doi.org/10.1002/9781118437865 (Chapter 5).

[14] S. Kermadi, S. Sali, F. Ait Ameur, L. Zougar, M. Boumaour, A. Toumiat, N.N. Melnik, D.W. Hewak, A. Duta, Effect of copper content and sulfurization process on optical, structural and electrical properties of ultrasonic spray pyrolysed Cu_2ZnSnS_4 thin films, Mater. Chem. Phys. 169 (2016) 96–104, http://dx.doi.org/10.1016/j.matchemphys.2015.11.035.

[15] A. Ashfaq, J. Jacob, N. Bano, M.A.U. Nabi, A. Ali, W. Ahmad, K. Mahmood, M.I. Arshad, S. Ikram, U. Rehman, N. Amin, S. Hussain, A two step technique to remove the secondary phases in CZTS thin films grown by sol–gel method, Ceram. Int. 45 (2019) 10876–10881, http://dx.doi.org/10.1016/j.ceramint.2019.02.165.

[16] J. Ge, J. Chu, J. Jiang, Y. Yan, P. Yang, Characteristics of In-substituted CZTS thin film and bifacial solar cell, ACS Appl. Mater. Interfaces 6 (2014) 21118–21130, http://dx.doi.org/10.1021/am505980n.

[17] F. Zhou, F. Zeng, X. Liu, F. Liu, N. Song, C. Yan, A. Pu, J. Park, K. Sun, X. Hao, Improvement of J_{sc} in a Cu_2ZnSnS_4 solar cell by using a thin carbon intermediate layer at the Cu_2ZnSnS_4/Mo interface, ACS Appl. Mater. Interfaces 7 (2015) 22868–22873, http://dx.doi.org/10.1021/acsami.5b05652.

[18] F. Liu, J. Huang, K. Sun, C. Yan, Y. Shen, J. Park, A. Pu, F. Zhou, X. Liu, J.A. Stride, M.A. Green, X. Hao, Beyond 8% ultrathin kesterite Cu_2ZnSnS_4 solar cells by interface reaction route controlling and self-organized nanopattern at the back contact, NPG Asia Mater. 9 (2017) e401, http://dx.doi.org/10.1038/am.2017.103.

[19] T. Shimada, F.S. Ohuchi, B.A. Parkinson, Thermal decomposition of SnS_2 and $SnSe_2$: novel molecular-beam epitaxy sources for sulfur and selenium, J. Vac. Sci. Technol. A: Vac. Surf. Films 10 (1992) 539–542, http://dx.doi.org/10.1116/1.578184.

[20] C. Khelia, K. Boubaker, M. Amlouk, SnxSy compounds growth by controlled sulfurisation of SnO_2, J. Alloys Compd.

509 (2011) 929–935,
http://dx.doi.org/10.1016/j.jallcom.2010.09.132.

[21] V. Piacente, S. Foglia, P. Scardala, Sublimation study of the tin sulphides SnS_2, Sn_2S_3 and SnS, J. Alloys Compd. 177 (1991) 17–30, http://dx.doi.org/10.1016/0925-8388(91)90053-X.

[22] T. Gürel, C. Sevik, T. Çağın, Characterization of vibrational and mechanical properties of quaternary compounds Cu_2ZnSnS_4 and $Cu_2ZnSnSe_4$ in kesterite and stannite structures, Phys. Rev. B 84 (2011) 205201, http://dx.doi.org/10.1103/PhysRevB.84.205201.

[23] A. Khare, B. Himmetoglu, M. Johnson, D.J. Norris, M. Cococcioni, E.S. Aydil, Calculation of the lattice dynamics and Raman spectra of copper zinc tin chalcogenides and comparison to experiments, J. Appl. Phys. 111 (2012) 083707, http://dx.doi.org/10.1063/1.4704191.

[24] B.G. Mendis, A.A. Taylor, M. Guennou, D.M. Berg, M. Arasimowicz, S. Ahmed, H. Deligianni, P.J. Dale, Nanometre-scale optical property fluctuations in Cu_2ZnSnS_4 revealed by low temperature cathodoluminescence, Solar Energy Mater. Sol. Cells 174 (2018) 65–76, http://dx.doi.org/10.1016/j.solmat.2017.08.028.

[25] M. Dimitrievska, A. Fairbrother, X. Fontané, T. Jawhari, V. Izquierdo-Roca, E. Saucedo, A. Pérez-Rodríguez, Multiwavelength excitation Raman scattering study of polycrystalline kesterite Cu_2ZnSnS_4 thin films, Appl. Phys. Lett. 104 (2014) 021901, http://dx.doi.org/10.1063/1.4861593.

[26] M. Paris, L. Choubrac, A. Lafond, C. Guillot-Deudon, S. Jobic, Solid-state NMR and Raman spectroscopy to address the local structure of defects and the tricky issue of the Cu/Zn disorder in Cu-poor, Zn-rich CZTS materials, Inorg. Chem. 53 (2014) 8646–8653, http://dx.doi.org/10.1021/ic5012346.

[27] A. Fairbrother, V. Izquierdo-Roca, X. Fontané, M. Ibáñez, A. Cabot, E. Saucedo, A. Pérez-Rodríguez, ZnS grain size effects on near-resonant Raman scattering: optical non-destructive grain size estimation, CrystEngCommun 16 (2014) 4120, http://dx.doi.org/10.1039/c3ce42578a.

[28] R. Martí Valls, T. Stoyanova Lyubenova, I. Calvet Roures, L. Oliveira, D. Fraga Chiva, J.B. Carda Castelló, Easy and low-cost aqueous precipitation method to obtain $Cu_2ZnSn(S, Se)_4$ thin layers, Sol. Energy Mater. Solar Cells 161 (2017) 432–438, http://dx.doi.org/10.1016/j.solmat.2016.12.031.

[29] P.A. Fernandes, P.M.P. Salomé, A.F. da Cunha, Growth and Raman scattering characterization of Cu_2ZnSnS_4 thin films, Thin Solid Films 517 (2009) 2519–2523, http://dx.doi.org/10.1016/j.tsf.2008.11.031.

[30] R.B.V. Chalapathy, G.S. Jung, B.T. Ahn, Fabrication of Cu_2ZnSnS_4 films by sulfurization of Cu/ZnSn/Cu precursor layers in sulfur atmosphere for solar cells, Sol. Energy Mater. Sol. Cells 95 (2011) 3216–3221, http://dx.doi.org/10.1016/j.solmat.2011.07.017.

[31] M.I. Khalil, R. Bernasconi, S. Ieffa, A. Lucotti, A. Le Donne, S. Binetti, L. Magagnin, Effect of Co-electrodeposited Cu–Zn–Sn precursor compositions on sulfurized CZTS thin films for solar cell, ECS Trans. 64 (2015) 33–41, http://dx.doi.org/10.1149/06429.0033ecst.

[32] N.R. Mathews, J. Tamy Benítez, F. Paraguay-Delgado, M. Pal, L. Huerta, Formation of Cu_2SnS_3 thin film by the heat treatment of electrodeposited SnS–Cu layers, J. Mater. Sci.: Mater. Electron. 24 (2013) 4060–4067, http://dx.doi.org/10.1007/s10854-013-1361-5.

[33] D. Courcot, C. Pruvost, E.A. Zhilinskaya, A. Aboukaïs, Potential of supported copper and potassium oxide catalysts in the combustion of carbonaceous particles, Kinet. Catal. 45 (2004) 580–588, http://dx.doi.org/10.1023/B:KICA.0000038089.98976.95.

[34] J. Wiley, New & Bestselling Books in Analytical Chemistry (n.d.) 1.

[35] Y. Huang, G. Li, Q. Fan, M. Zhang, Q. Lan, X. Fan, Z. Zhou, C. Zhang, Facile solution deposition of Cu_2ZnSnS_4 (CZTS) nano-worm films on FTO substrates and its photoelectrochemical property, Appl. Surf. Sci. 364 (2016) 148–155, http://dx.doi.org/10.1016/j.apsusc.2015.12.065.

[36] G. Gordillo, C. Calderón, P. Bartolo-Pérez, XPS analysis and structural and morphological characterization of Cu_2ZnSnS_4 thin films grown by sequential evaporation, Appl. Surf. Sci. 305 (2014) 506–514, http://dx.doi.org/10.1016/j.apsusc.2014.03.124.

[37] N. Song, M.A. Green, J. Huang, Y. Hu, X. Hao, Study of sputtered Cu_2ZnSnS_4 thin films on Si, Appl. Surf. Sci. 459 (2018) 700–706, http://dx.doi.org/10.1016/j.apsusc.2018.07.192.

[38] S.K. Wallace, D.B. Mitzi, A. Walsh, The steady rise of kesterite solar cells, ACS Energy Lett. 2 (2017) 776–779, http://dx.doi.org/10.1021/acsenergylett.7b10013.

[39] S. Siebentritt, G. Rey, A. Finger, D. Regesch, J. Sendler, T.P. Weiss, T. Bertram, What is the bandgap of kesterite? Sol. Energy Mater. Sol. Cells 158 (2016) 126–129, http://dx.doi.org/10.1016/j.solmat.2015.10.017.

[40] J. Henry, K. Mohanraj, G. Sivakumar, Electrical and optical properties of CZTS thin films prepared by SILAR method, J. Asian Ceram. Soc. 4 (2016) 81–84, http://dx.doi.org/10.1016/j.jascer.2015.12.003.

[41] E.A. Kraut, R.W. Grant, J.R. Waldrop, S.P. Kowalczyk, Precise determination of the valence-band edge in X-ray photoemission spectra: application to measurement of semiconductor interface potentials, Phys. Rev. Lett. 44 (1980) 1620–1623, http://dx.doi.org/10.1103/PhysRevLett.44.1620.

[42] E.A. Kraut, R.W. Grant, J.R. Waldrop, S.P. Kowalczyk, Semiconductor core-level to valence-band maximum binding-energy differences: precise determination by X-ray photoelectron spectroscopy, Phys. Rev. B 28 (1983) 1965–1977, http://dx.doi.org/10.1103/PhysRevB.28.1965.

[43] M. Bär, B.-A. Schubert, B. Marsen, R.G. Wilks, S. Pookpanratana, M. Blum, S. Krause, T. Unold, W. Yang, L. Weinhardt, C. Heske, H.-W. Schock, Cliff-like conduction band offset and KCN-induced recombination barrier enhancement at the CdS/Cu_2ZnSnS_4 thin-film solar cell heterojunction, Appl. Phys. Lett. 99 (2011) 222105, http://dx.doi.org/10.1063/1.327 3663.